

Biochemical Characterization of the Catalytic Domain of Human Matrix Metalloproteinase 19

EVIDENCE FOR A ROLE AS A POTENT BASEMENT MEMBRANE DEGRADING ENZYME*

Received for publication, December 21, 1999, and in revised form, January 31, 2000

Jan O. Stracke‡§, Mike Hutton‡, Margaret Stewart‡, Alberto M. Pendás¶, Bryan Smith||, Carlos López-Otin¶, Gillian Murphy‡, and Vera Knäuper‡

From the ‡School of Biological Sciences, University of East Anglia, Norwich, NR4 7TJ, United Kingdom, the ¶Departamento de Bioquímica y Biología Molecular, Universidad de Oviedo, 33006 Oviedo, Spain, and ||Celltech Chiroscience Ltd., 216 Bath Road, Slough SL1 4EN, United Kingdom

We have recently cloned MMP-19, a novel **matrix metalloproteinase**, which, due to unique structural features, was proposed to represent the first member of a new MMP subfamily (Pendás, A. M., Knäuper, V., Puente, X. S., Llano, E., Mattei, M. G., Apte, S., Murphy, G., and López-Otin, C. (1997) *J. Biol. Chem.* 272, 4281–4286). A recombinant COOH-terminal deletion mutant of MMP-19 (pro $\Delta_{260-508}$ MMP-19), comprising the propeptide and the catalytic domain, was expressed in *Escherichia coli*, refolded, and purified. Interestingly, we found that pro $\Delta_{260-508}$ MMP-19 has the tendency to autoactivate, whereby the Lys⁹⁷-Tyr⁹⁸ peptide bond is hydrolyzed, resulting in free catalytic domain. Mutation of two residues (Glu⁸⁸ \rightarrow Pro and Pro⁹⁰ \rightarrow Val) within the propeptide latency motif did not prevent autoactivation but the autolysis rate was somewhat reduced. Analysis of the substrate specificity revealed that the catalytic domain of MMP-19 was able to hydrolyze the general MMP substrate Mca-Pro-Leu-Gly-Dpa-Ala-Arg-NH₂ and, with higher efficiency, the stromelysin substrate Mca-Pro-Leu-Ala-Nva-Dpa-Ala-Arg-NH₂. Kinetic analysis of the interactions of the catalytic domain of MMP-19 with the natural MMP inhibitors, the tissue inhibitors of metalloproteinases (TIMPs), showed strong inhibition using TIMP-2, TIMP-3, and TIMP-4, while TIMP-1 was less efficient. We also demonstrated that synthetic hydroxamic acid-based compounds efficiently inhibited the enzyme. The catalytic domain of MMP-19 was able to hydrolyze the basement membrane components type IV collagen, laminin, and nidogen, as well as the large tenascin-C isoform, fibronectin, and type I gelatin *in vitro*, suggesting that MMP-19 is a potent proteinase capable of hydrolyzing a broad range of extracellular matrix components. Neither the catalytic domain nor the full-length MMP-19 was able to degrade triple-helical collagen. Finally, and in contrast to studies with other MMPs, MMP-19 catalytic domain was not able to activate any of the latent MMPs tested *in vitro*.

The human matrix metalloproteinases (MMPs)¹ are a group

* This work was supported by Arthritis Research Campaign Grant K0541, by German Academic Exchange Service Studentship Grant D/97/2127, and by the Wellcome Trust. The costs of publication of this article were defrayed in part by the payment of page charges. This article must therefore be hereby marked "advertisement" in accordance with 18 U.S.C. Section 1734 solely to indicate this fact.

§ To whom correspondence should be addressed: School of Biological Sciences, University of East Anglia, Norwich NR4 7TJ, United Kingdom. Tel.: 44-1603-593829; Fax: 44-1603-592250; E-mail: j.stracke@uea.ac.uk.

¹ The abbreviations used are: MMP, matrix metalloproteinase; TIMP,

of homologous zinc-dependent endopeptidases that degrade the different macromolecular components of the extracellular matrix. They have been implicated in the remodeling of connective tissues during such diverse processes as normal mammalian development and growth, wound healing, cartilage degradation during arthritis, and cancer metastasis (1–3). At present 18 members of the human MMP family have been cloned, and they have been classified into different subfamilies according to their substrate specificity and cellular location. This classification comprises the collagenases, gelatinases, stromelysins, and membrane-type MMPs (MT-MMPs). We have recently cloned a new member of the matrix metalloproteinase family, MMP-19, which showed the typical domain organization of soluble members of the MMP family, namely a signal sequence, a propeptide domain with the cysteine residue essential for maintaining latency, a catalytic domain with the typical zinc binding motif, a linker region, and a COOH-terminal fragment with sequence similarity to hemopexin (4). However, the enzyme lacks various structural features distinctive of the diverse MMP subfamilies, e.g. the fibronectin-like repeats of gelatinases or the Asp, Tyr, and Gly residues near the active site of collagenases, but possesses a unique insertion of five Glu residues within the linker region, an unusual latency motif in the propeptide domain (. . . PRCGLEDP . . .) and an additional Cys residue in the catalytic domain, when compared with other MMPs. In addition, the MMP-19 gene is the first MMP gene found to be located on chromosome locus 12q14 and initial data on its genomic organization has revealed a unique intron/exon distribution. MMP-19 may therefore represent the first member of a new subfamily of MMPs (4), whose role *in vivo* remains to be investigated. However, recently, MMP-19 mRNA was found to be constitutively expressed in arthritic (RA) and traumatic synovial membranes, which may imply the involvement of MMP-19 in this tissue during normal ECM remodeling processes (5). Northern blot analysis of polyadenylated RNA from various normal human tissues revealed strong expression of MMP-19 in placenta, ovary, lung, pancreas, spleen, and intestine, whereas expression in brain and leukocytes was undetectable (4). Since adult cells under non-pathological conditions do not frequently produce MMPs, it is possible that MMP-19 participates in normal ECM turnover or in activation of secreted and membrane-bound proteins such as growth factors and protein-

tissue inhibitor of metalloproteinase; ECM, extracellular matrix; RA, rheumatoid arthritis; Mca, (7-methoxycoumarin-4-yl)-acetyl; Cha, 3-cyclohexylalanyl; Nva, norvalyl; Dpa, *N*-3-(2,4-dinitrophenyl)-L-2,3-diaminopropionyl; Dnp, 2,4-dinitrophenyl; APMA, *p*-aminophenylmercuric acetate; PAGE, polyacrylamide gel electrophoresis; PCR, polymerase chain reaction; MT, membrane-type; MES, 4-morpholineethanesulfonic acid; CAPS, 3-(cyclohexylamino)propanesulfonic acid.

ases (4). More recently, Sedlacek and co-workers (6) reported that enhanced anti-MMP-19 autoantibody titers appear to be frequent among patients suffering from RA, and that MMP-19 was detected using an anti-peptide antibody on the surface of lymphatic cells such as activated peripheral blood mononuclear cells, T_H1 lymphocytes, and Jurkat T lymphoma cells. Furthermore, a distinct expression of MMP-19 was observed, associated with the smooth muscle cells in the tunica media of synovial blood vessels of an RA patient, as well as in normal skin and uterine ligaments (7). In contrast, in capillaries of acutely inflamed RA synovium strong MMP-19 expression was also detected in the endothelial layer (8). The same authors report an elevated MMP-19 mRNA expression of smooth muscle cells *in vitro* after stimulation with 12-*O*-tetradecanoylphorbol-13-acetate, epidermal growth factor, and basic fibroblast growth factor, whereby proliferating smooth muscle cells exhibited higher levels of MMP-19 mRNA than resting cells. MMP-19 protein and mRNA was detected *in vitro* in endothelial cells from various tissues, *e.g.* umbilical artery, skin, and fat tissue. These data support the hypothesis that MMP-19 participates in angiogenic processes and lymphocyte extravasation during arthritic diseases and therefore may be involved in the invasion of the inflamed synovial pannus into the joint space and thus in the destruction of joint tissues. Here we describe the expression, refolding, and enzymatic characterization of the catalytic domain of MMP-19.

EXPERIMENTAL PROCEDURES

Expression, Refolding, and Purification of Pro $\Delta_{260-508}$ MMP-19—An expression vector for pro $\Delta_{260-508}$ MMP-19 was generated by PCR using the following primers: 5'-GGGCCTGCAGACTACCTGTACAATATGGGTACCTACAGAGCC-3' (A) and 5'-CCGGAATCTCAACTCTTCTTGCATAGAGACTGGATCCCTGC-3' (B) using the full-length MMP-19 cDNA in pSP64 as a template, thereby introducing a *Pst*I site at the 5' end and a stop codon following Ser²⁵⁹ flanked by a unique *Eco*RI site at the 3' end of the PCR product. The 800-bp PCR product was cleaved with the restriction endonucleases *Pst*I and *Eco*RI and ligated in frame into the pRSET B expression vector (Invitrogen), thereby adding an NH₂-terminal His₆ tag to the protein. The correct sequence of the pro $\Delta_{260-508}$ MMP-19 cDNA was confirmed by double-strand dideoxy sequencing. The expression of pro $\Delta_{260-508}$ MMP-19 as inclusion bodies in competent BL21(DE3)pLysS *E. coli* cells was carried out as described previously (4). The inclusion bodies were solubilized in 20 mM Tris/H₂SO₄, pH 8.0, 6 mM urea, 5 mM β -mercaptoethanol, 0.01% Na₃N at 37 °C for 30 min. Refolding was achieved by dilution (1:250) into 20 mM Tris/H₂SO₄, pH 7.6, 100 mM Na₂SO₄, 5 mM CaSO₄, 5 μ M ZnSO₄, 5% glycerol, 0.03% Brij 35 (w/v), 0.01% Na₃N at 4 °C. The refolding mixture was filtered and applied to a nickel-nitrilotriacetic acid-agarose column (Qiagen) equilibrated in above buffer. Under these conditions, the protein bound via the NH₂-terminal His₆ tag to the column and was washed with above buffer containing 5 mM imidazole. The protein was eluted with buffer supplemented with 100 mM imidazole. After SDS-PAGE analysis, fractions containing pro $\Delta_{260-508}$ MMP-19 were combined and dialyzed against 20 mM Tris/HCl, pH 7.6, 200 mM NaCl, 5 mM CaCl₂, 0.03% Brij 35 (w/v), 0.01% Na₃N, followed by centrifugation to remove precipitated protein and concentration in an Amicon concentrator with a *M_r* 10,000 cut-off cartridge. All buffers used for refolding and purification contain an EDTA-free protease inhibitor mixture at concentrations recommended by the supplier (Roche Molecular Biochemicals).

Mutagenesis of Pro $\Delta_{260-508}$ MMP-19—To alter two sequence motifs within pro $\Delta_{260-508}$ MMP-19 site-directed mutagenesis was performed using the method of Ho *et al.* (9). The mutations were located in the propeptide (E88P/P90V) and in the catalytic domain (C166S).

The mutants E88P/P90V and C166S were generated by PCR using the following primer pairs: 5'-CTACCGGATGCTTCAACCAGAGACCTTAAA-3' (C) with 5'-GAAGACATCCGGTAGGCCACAACGAGGCTGCCT-3' (D), and 5'-CGTACTCGTCCAATACTTTTGATGGGCCTG-3' (E) with 5'-TTGGACGAGTACGAGCTTTGGCGGCCATGG-3' (F), respectively, in combination with primers A and B from above. Subcloning, expression, refolding, and purification were performed as described for the wild type pro $\Delta_{260-508}$ MMP-19.

A protein containing alterations in both, propeptide and catalytic

domain, was produced, thereby altering E88P/P90V and C166S by ligating the *Pst*I and *Nco*I fragment from pro $\Delta_{260-508}$ MMP-19(E88P/P90V) into the pRSET B vector containing the mutation for C166S in the catalytic domain, previously cleaved with the same restriction enzymes. Expression and refolding were performed as described above. All expression vectors were sequenced using the dideoxy chain termination method and confirmed the correct sequence for each construct.

Expression and Purification of Full-length MMP-19—Human MMP-19 was purified from culture medium conditioned by NS0 mouse myeloma cells that had been transfected with MMP-19 cDNA, essentially as described previously (10). The expression vector, transfection method, and culture conditions were as described previously (11, 12).

Expression and Purification of Recombinant TIMPs—Recombinant forms of human TIMP-1, -2, and -3 were generated as described previously (11–13). TIMP-4 was expressed and purified from bacterial inclusion bodies, essentially as reported for TIMP-2 (14). Generation of wild type $\Delta_{128-194}$ TIMP-2 and the $\Delta_{128-194}$ TIMP-2 mutants S2E, Y36G, and A70K was performed as described previously (15).

Activity Assays, Active Site Titration, and Kinetic Analysis of Inhibitor Binding—Enzymatic activity was determined after activation of wild type or mutated pro $\Delta_{260-508}$ MMP-19 with 1 mM APMA for 30 min at 37 °C (16). Routine assays were performed at 37 °C using 1 mM enzyme and the synthetic quenched fluorescent peptide (7-methoxycoumarin-4-yl)acetyl-Pro-Leu-Ala-Nva-[3-(2, 4-dinitrophenyl)-L-2,3-diaminopropionyl]-Ala-Arg-NH₂ (λ_{ex} 328 nm, λ_{em} 393 nm) as substrate at a concentration of 1 μ M in assay buffer (50 mM Tris/HCl, pH 7.6, 150 mM NaCl, 10 mM CaCl₂, 0.05% (v/v) Brij 35, 0.01% Na₃N). The concentration of active enzyme was evaluated using the fluorescent assay by titration against a standard TIMP-2 solution of known concentration (12). Determination of the substrate specificity of the catalytic domain of MMP-19 was carried out using the same assay with different quenched fluorescent synthetic peptide substrates at concentrations of 1 μ M, which fulfilled the requirements of [S] \ll *K_m*. All peptide substrates were kindly provided by Dr. Graham Knight (University of Cambridge, Cambridge, United Kingdom). The pseudo-first-order rate constants (*k*) for the formation of the EI complex of 1 nM active wild type $\Delta_{260-508}$ MMP-19 with TIMP-1, -2, -3, and -4, and the $\Delta_{128-194}$ TIMP-2 mutants S2E, Y36G, and A70K were determined by analysis of the progress curves of McaPLANvaDpaARNH₂ hydrolysis (12). The dependence of *k* on TIMP concentration was evaluated using various amounts of TIMP (5–20 nM). In addition, the apparent *K_i^{app}* values for TIMP inhibition were determined using 1 nM enzyme incubated with a range of inhibitor concentrations for 24 h at 37 °C to reach equilibrium before assayed as described above.

The apparent *K_i* values for the inhibition of active wild type $\Delta_{260-508}$ MMP-19 with the synthetic hydroxamic acid-based inhibitors CT-1746, Ro31-9790, and BB-94 were determined by incubation of 1 nM enzyme with a range of inhibitor concentrations for 24 h at 37 °C before assayed.

pH Dependence of $\Delta_{260-508}$ MMP-19 Activity—The pH dependence of the activity of $\Delta_{260-508}$ MMP-19 was determined at 37 °C, after complete activation with 1 mM APMA for 30 min, using 1 nM enzyme and 1 μ M synthetic fluorescent substrate McaPLANvaDpaARNH₂ in a buffer of 20 mM MES, 20 mM Tris, 20 mM CAPS, 150 mM NaCl, 10 mM CaCl₂, 0.05% (v/v) Brij 35. The pH was adjusted with HCl in steps of 0.5 before every measurement, covering a range from pH 5 to pH 11.

Cleavage of Extracellular Matrix Components—A wide variety of extracellular matrix molecules such as collagen type I, gelatin type I, collagen type IV, laminin, nidogen, fibronectin, tenascin-C (small and large isoforms), fibrin, and fibrinogen were incubated in time-course experiments at 37 °C (if not stated otherwise) with active $\Delta_{260-508}$ MMP-19 prior to analysis by SDS-PAGE. Type I collagen was prepared from rat skin, as described previously (17). Tenascin-C small and large isoforms were obtained from baby hamster kidney cells transfected with tenascin-C cDNA constructs (18). Mouse laminin, human fibronectin and human fibrinogen were purchased from Sigma. Collagen type IV and nidogen were generous gifts from Klaus Kühn and Rupert Timpl, respectively. Fibrin was generated from fibrinogen by clotting with thrombin prior to incubation with active $\Delta_{260-508}$ MMP-19 (19). Monoclonal antibodies to fibronectin domains were purchased from Life Technologies, Inc. Human recombinant stromelysin-1 (MMP-3) and gelatinase A (MMP-2), which were used as a comparison, were prepared as described previously and activated by trypsin and APMA, respectively (20, 21). The enzyme/substrate ratio (w/w) used in these experiments was 1/10. Furthermore, ¹⁴C-labeled gelatin and casein were used in an assay described by Cawston and Barrett (17) to quantify the specific catalytic activity of wild type $\Delta_{260-508}$ MMP-19 hydrolyzing these molecules. Gelatin and casein zymography was per-

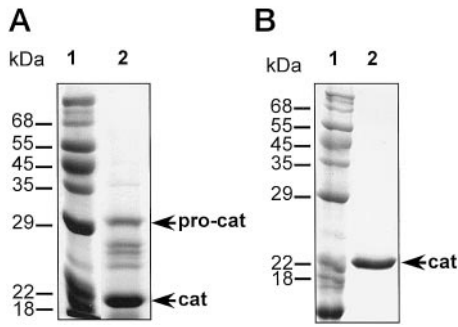


FIG. 1. SDS-PAGE analysis of purified recombinant pro $\Delta_{260-508}$ MMP-19 produced by bacterial cells. Panel A, lane 1, molecular size standard; lane 2, purified pro $\Delta_{260-508}$ MMP-19, processing from the latent to the active form. Panel B, lane 1, molecular size standard; lane 2, active $\Delta_{260-508}$ MMP-19. Molecular mass markers are indicated on the left. The latent and active forms of the mutants pro $\Delta_{260-508}$ MMP-19(C166S), pro $\Delta_{260-508}$ MMP-19(E88P/P90V), and pro $\Delta_{260-508}$ MMP-19(C166S/E88P/P90V) display the same masses as wild type pro $\Delta_{260-508}$ MMP-19 (data not shown).

formed as described previously (22).

Activation of Other Matrix Metalloproteinases by Active $\Delta_{260-508}$ MMP-19—The proenzymes of human collagenase-1 (MMP-1), gelatinase A (MMP-2), stromelysin-1 (MMP-3), neutrophil collagenase (MMP-8), gelatinase B (MMP-9), collagenase-3 (MMP-13), and MT1-MMP (MMP-14) were incubated for 24 h with active $\Delta_{260-508}$ MMP-19 at a 1:1 (w/w) ratio of enzyme versus substrate at 37 °C in 50 mM Tris/HCl, pH 7.6, 150 mM NaCl, 10 mM CaCl₂, 0.05% (v/v) Brij 35. Aliquots of the reaction mixture were removed at the time intervals indicated and analyzed by SDS-PAGE. The processing of pro-gelatinase B by active $\Delta_{260-508}$ MMP-19 was further assessed in time-course experiments at 37 °C with 1:10 ratio (w/w) of $\Delta_{260-508}$ MMP-19 and proMMP-9 in the above buffer. Aliquots of the reaction mixture were removed at the time intervals indicated, diluted to a final enzyme concentration of 25 μ M, and assayed for activity in the fluorimeter using the synthetic quenched fluorescent peptide substrate (7-methoxycoumarin-4-yl)acetyl-Pro-Leu-Gly-Leu-[3-(2, 4-dinitrophenyl)-L-2,3-diaminopropionyl]-Ala-Arg-NH₂ (λ_{ex} 328 nm, λ_{em} 393 nm) at a concentration of 1 μ M. Molecular mass changes were monitored by SDS-PAGE and silver staining.

NH₂-terminal Sequence Determination—Proteins were purified by reverse phase high performance liquid chromatography using a C₁₈-column followed by automated Edman degradation using a PE Biosystems 492 Precise protein sequencer operated according to manufacturer's instructions.

RESULTS AND DISCUSSION

Human MMP-19 is a novel member of the matrix metalloproteinase family, cloned recently from a human liver cDNA library (4). Consequently, biochemical analysis of the activation mechanism, substrate specificity, and inhibition profile of MMP-19 is of vital importance in order to understand its possible function *in vivo* and to design specific inhibitors as potential new therapeutic agents. Since purification of full-length MMP-19 expressed in mammalian and bacterial expression systems resulted in low yields, autoproteolytic activation, and partial fragmentation, we decided to use the COOH-terminal truncated form of MMP-19, pro $\Delta_{260-508}$ MMP-19 (numbering starts at Met¹, GenBank™/EBI accession number X92521), for this study and analyzed its enzymatic properties.

Refolding, Purification, and Activation of Pro $\Delta_{260-508}$ MMP-19, and Assessment of Mutations within the Pro and Catalytic Domains—In order to further characterize the catalytic activity of MMP-19, we expressed and refolded the COOH-terminal truncated form of MMP-19, pro $\Delta_{260-508}$ MMP-19, comprising the pro and catalytic domains, and analyzed the protein biochemically in detail. After solubilization and refolding, pro $\Delta_{260-508}$ MMP-19 was purified using nickel-nitrilotriacetic acid-agarose and the eluted proenzyme displayed the expected mass of 30 kDa when analyzed by SDS-PAGE (Fig. 1A). Surprisingly, following dialysis to remove the imidazole, all the

enzyme autoactivated, resulting in the generation of active enzyme with a mass of 20 kDa under reducing conditions (Fig. 1B). NH₂-terminal amino acid sequence determination of the active catalytic domain confirmed that the Lys⁹⁷-Tyr⁹⁸ peptide bond was hydrolyzed during autoproteolytic activation (Fig. 2).

Similar autoactivation was observed when we attempted to purify full-length MMP-19 from the culture medium of stable transfected NS0 cells (data not shown). In order to define the residues in the proenzyme that make proMMP-19 prone to autoactivation, we performed site-directed mutagenesis experiments by targeting the latency motif PRGGL⁸⁸DP⁹⁰ of proMMP-19 and the residue Cys¹⁶⁶ in the catalytic domain, which are structural elements different from other MMPs. The mutants pro $\Delta_{260-508}$ MMP-19(C166S), pro $\Delta_{260-508}$ MMP-19(E88P/P90V), and pro $\Delta_{260-508}$ MMP-19(C166S/E88P/P90V) were expressed, solubilized, refolded, and purified in the same way as described for the wild type pro $\Delta_{260-508}$ MMP-19. All mutants are of the same size as wild type when analyzed by SDS-PAGE and activate spontaneously during refolding and purification (Fig. 1 and data not shown). However, the tendency to undergo activation is slowed down by approximately 50% for the two mutants pro $\Delta_{260-508}$ MMP-19(E88P/P90V) and pro $\Delta_{260-508}$ MMP-19(C166S/E88P/P90V), confirming previously published data, where the effects of single mutations within the latency motif of transin (rat stromelysin) upon activation were reported (23). In both of these pro $\Delta_{260-508}$ MMP-19 mutants, the alterations reestablish the sequence PRGVPDV, conserved within the propeptide of MMPs. Thus, our results suggest that the tendency of pro $\Delta_{260-508}$ MMP-19 and full-length MMP-19 to undergo autoactivation can be ascribed partially to its unique latency motif. Cys¹⁶⁶ within the catalytic domain seems not to influence activation and its function remains unclear. However, we observed low amounts of dimers of active recombinant wild type $\Delta_{260-508}$ MMP-19 by casein zymography and SDS-PAGE, whereas the mutants containing C166S did not form any dimers under the same conditions (data not shown). There is no *in vivo* evidence, however, that the residue Cys¹⁶⁶ facilitates dimerization or linkage to other proteins.

If not stated otherwise, we used the active wild type catalytic domain of MMP-19 (active $\Delta_{260-508}$ MMP-19) for further biochemical characterization.

Kinetic Analysis of Cleavage of Quenched Fluorescent Substrates and TIMP Binding—In order to assess the substrate specificity of active $\Delta_{260-508}$ MMP-19 further, seven synthetic quenched fluorescent peptide substrates were employed (Table I). Only the general MMP substrate Mca-Pro-Leu-Gly-Dpa-Ala-Arg-NH₂ and the stromelysin substrate Mca-Pro-Leu-Ala-Nva-Dpa-Ala-Arg-NH₂ were hydrolyzed efficiently, while other substrates were resistant to hydrolysis, thus confirming our preliminary data (4). The k_{cat}/K_m values obtained for these two substrates are in agreement with our earlier results. Therefore, the catalytic domain of MMP-19 has a substrate specificity similar to that for the stromelysin subfamily of MMPs since it preferably hydrolyzed Mca-Pro-Leu-Ala-Nva-Dpa-Ala-Arg-NH₂, which was designed as a substrate to study stromelysin activity. However, stromelysin-1 (MMP-3) hydrolyzes both substrates, Mca-Pro-Leu-Gly-Dpa-Ala-Arg-NH₂ and Mca-Pro-Leu-Ala-Nva-Dpa-Ala-Arg-NH₂, more efficiently than active $\Delta_{260-508}$ MMP-19 (20).

Furthermore, we followed $\Delta_{260-508}$ MMP-19 activity over a wide pH range (pH 5.0–11.0) using a constant enzyme concentration of 1 nM and Mca-Pro-Leu-Ala-Nva-Dpa-Ala-Arg-NH₂ as substrate in the quenched fluorescent assay (Fig. 3). The activity, measured in steps of 0.5, showed low k_{cat}/K_m values at pH 5.0 and a sudden increase toward pH 7.0, where the highest

FIG. 2. NH₂-terminal sequence determination of pro $\Delta_{260-508}$ MMP-19 in pRSET B and active $\Delta_{260-508}$ MMP-19. The NH₂ terminus of active $\Delta_{260-508}$ MMP-19 is indicated with an arrow. The numbering of the amino acid sequence starts with Met¹.

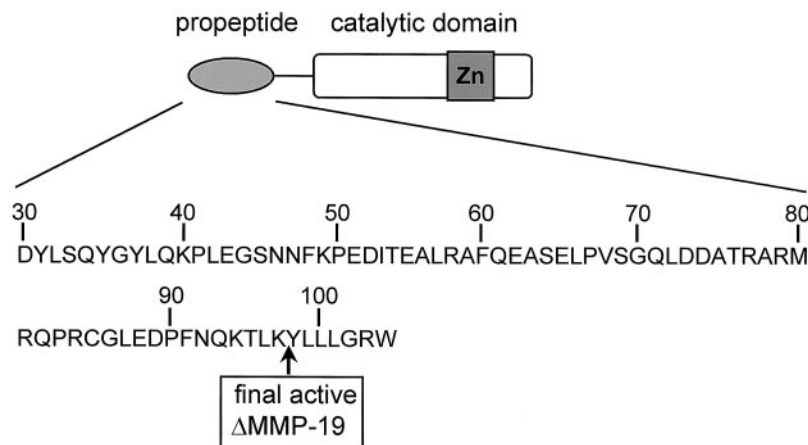


TABLE I

Substrate specificity of active $\Delta_{260-508}$ MMP-19: k_{cat}/K_m values for various synthetic quenched fluorescent substrates at 37 °C.

1, general MMP substrate; 2, stromelysin substrate; 3, substrate based on the α_2 -macroglobulin bait region; 4, collagenase substrate; 5, substrate based on the aggrecanase cleavage site; 6, TNF- α convertase substrate; 7, substrate based on the myelin basic protein cleavage site generated by the disintegrin metalloproteinase (MADAM).

Substrate	k_{cat}/K_m
	M^{-1}/s^{-1}
1. Mca-Pro-Leu-Gly-Dpa-Ala-Arg-NH ₂	1.93×10^3
2. Mca-Pro-Leu-Ala-Nva-Dpa-Ala-Arg-NH ₂	3.09×10^4
3. Mca-Pro-Glu-Gly-Leu-Arg-Dpa-NH ₂	Not cleaved
4. Mca-Pro-Cha-Gly-Nva-His-Ala-Dpa-NH ₂	Not cleaved
5. Mca-Thr-Glu-Gly-Glu-Ala-Arg-Gly-Ser-Dpa-NH ₂	Not cleaved
6. Mca-Ser-Pro-Leu-Ala-Gln-Ala-Val-Arg-Ser-Ser-Ser-Arg-Lys(Dpn)-NH ₂	Not cleaved
7. Mca-His-Tyr-Gly-Ser-Leu-Pro-Gln-Lys-Ser-His-Gly-Arg-Lys(Dpn)-D-Arg-OH	Not cleaved

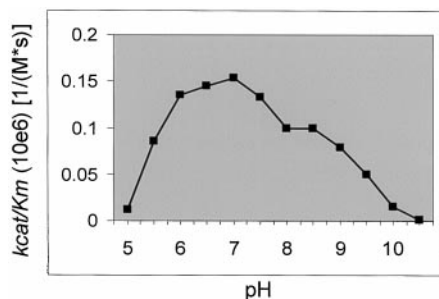


FIG. 3. Determination of the pH dependence of $\Delta_{260-508}$ MMP-19 activity in the fluorescent assay. k_{cat}/K_m values were obtained at 37 °C using 1 nM enzyme and the synthetic quenched fluorescent substrate Mca-Pro-Leu-Ala-Nva-Dpa-Ala-Arg-NH₂ at 1 μ M.

value was obtained, followed by a gradual decrease toward pH 10.5, where no activity was measurable. Thus, MMP-19 is active over a wide pH range and displays maximum activity at pH 7.0 in our assay. A comparison of the pH profiles of MMP-19 and MMP-3 reveals that the latter seems to prefer a more acidic environment, reaching maximum activity at pH 6.0 (24).

The apparent K_i values for the inhibition of active $\Delta_{260-508}$ MMP-19 with the various TIMPs were determined using a constant enzyme concentration of 1 nM in the quenched fluorescent assay at 37 °C with Mca-Pro-Leu-Ala-Nva-Dpa-Ala-Arg-NH₂ as substrate (Table II). Under these conditions, only the K_i^{app} for TIMP-1 was determined with accuracy, since its value (57.6 nM) is well above the employed enzyme concentration and represents the weakest value ascertained for full-length TIMPs. In contrast, the K_i^{app} for TIMP-2, TIMP-3, and TIMP-4 were all in the range of 4–5 pM and are only rough estimates of the true values, because we were not able to determine them using enzyme concentrations below K_i^{app} due to the lack of assay sensitivity. However, the K_i^{app} values in the picomolar range indicate very strong enzyme-inhibitor interactions.

TABLE II

Kinetic analysis of the inhibition of MMP-19 catalytic domain by various TIMPs

k_{on} , association rate constant; K_i^{app} , apparent dissociation constant of the enzyme/inhibitor complex. All values were measured at 37 °C.

Inhibitor	$k_{on} (\times 10^4)$	K_i^{app}
	$M^{-1}s^{-1}$	(pM)
TIMP-1	1.22	57,600 (\pm 6.995)
TIMP-3	3.049	<5
TIMP-4	13.0 (\pm 2.5)	<5
TIMP-2	41.8 (\pm 3.5)	<5
$\Delta_{128-194}$ TIMP-2	10.2 (\pm 1.9)	14 (\pm 7)
$\Delta_{128-194}$ TIMP-2 (Y36G)	13.8 (\pm 0.49)	24.2 (\pm 9)
$\Delta_{128-194}$ TIMP-2 (A70K)	16.0 (\pm 2.7)	745.5 (\pm 69)
$\Delta_{128-194}$ TIMP-2 (S2E)	1.05 (\pm 0.34)	61,570 (\pm 4337)

The same restrictions apply to the K_i^{app} for the interactions of COOH-terminal truncated forms of enzyme and inhibitor, active $\Delta_{260-508}$ MMP-19 and $\Delta_{128-194}$ TIMP-2, which also result in values within the picomolar range and are, thus, not accurate. In addition, we investigated the inhibitory potential of mutants of $\Delta_{128-194}$ TIMP-2, containing single amino acid changes, with the aim to determine the sites in the NH₂-terminal, inhibitory region of TIMP-2, which are important for interactions with MMP-19 (Table II). From the three mutants used in this study, Y36G, A70K and S2E, only A70K (745 pM) and S2E (61.57 nM) show a marked decrease in affinity for the enzyme. In particular, the mutation S2E results in a dramatic decline of the inhibitory potential when compared with the wild type $\Delta_{128-194}$ TIMP-2.

Furthermore, the association rate of enzyme and inhibitor complex formation were assessed by measuring the curvature in the progress curve of substrate hydrolysis and analyzed as described previously (Table II) (25). The k_{on} values obtained were $1.22 \times 10^4 M^{-1} s^{-1}$ for TIMP-1, and $3.049 \times 10^4 M^{-1} s^{-1}$ for TIMP-3. In comparison, the association of TIMP-2 and

TABLE III

Kinetic analysis of the inhibition of MMP-19 catalytic domain by three hydroxamate-based inhibitors and comparison to stromelysin-1 (MMP-3)

K_i^{app} , apparent dissociation constant of enzyme/inhibitor complex; BB-94, general MMP inhibitor; Ro31-9790, weak stromelysin-1 inhibitor ($K_i^{app} \sim 100$ nM); CT-1746, weak collagenase-1 inhibitor ($K_i^{app} \sim 100$ nM). All values were measured at 37 °C.

Inhibitor	K_i^{app}	
	$\Delta_{260-508}$ MMP-19	MMP-3
	(nM)	
BB-94	0.06	2.0
Ro31-9790	1.2	119
CT-1746	0.05	10.9

TIMP-4 with the enzyme were considerably faster (4.18×10^5 and 1.3×10^5 $M^{-1} s^{-1}$, respectively). TIMP-4 shows similar features in the inhibition of the catalytic domain of MMP-19 as TIMP-2, the strongest known inhibitor for MMP-19 (4), which is in agreement with the high homology between these two inhibitors (26). Interestingly, the interaction of the catalytic domain of MMP-19 with TIMP-2 was found to be about 4 times faster than the one observed with the COOH-terminal deletion mutant $\Delta_{128-194}$ TIMP-2 (4.18×10^5 $M^{-1} s^{-1}$ and 1.02×10^5 $M^{-1} s^{-1}$, respectively), suggesting an influence of the COOH terminus of TIMP-2 on the association with active $\Delta_{260-508}$ MMP-19, which is in agreement with our previous data on the domain interactions involved in the binding of TIMPs to MMPs and suggestions from recent crystallographic analysis of the MT1-MMP/TIMP-2 complex (12, 25, 27). However, the small differences in K_i^{app} observed between TIMP-2 and $\Delta_{128-194}$ TIMP-2 (both picomolar) confirm that the NH₂-terminal domain of TIMP-2 alone is able to form stable complexes with the enzyme and, thus, is sufficient for the inhibition of MMP-19 (Table II). These results are confirmed by data on the interactions of $\Delta_{128-194}$ TIMP-2 with MMP-3 (28).

The $\Delta_{128-194}$ TIMP-2 mutants Y36G and A70K do not show a significant change of association if compared with the wild type $\Delta_{128-194}$ TIMP-2. However, the mutation S2E slows down the association of active $\Delta_{260-508}$ MMP-19 and inhibitor with 1 order of magnitude (1.05×10^4 $M^{-1} s^{-1}$), and results in a 10,000-fold increase in K_i^{app} (61.57 nM), therefore weakening the inhibitory properties considerably. In case of A70K, merely the K_i^{app} was increased about 50 times when compared with the wild type $\Delta_{128-194}$ TIMP-2, whereas the association rate constant was unchanged. From our data we can deduce that both mutations, A70K and S2E, result in increased enzyme-inhibitor complex dissociation, suggesting that the exchange of these amino acids compromise vital enzyme-inhibitor interactions. We therefore conclude that for the formation of the enzyme-inhibitor complex, similar to other MMPs, $\Delta_{260-508}$ MMP-19 interacts with the so-called "ridge" region in TIMP-2 (Cys¹-Cys³ and Ser⁶⁸-Cys⁷²) (15, 27, 29–32).

Kinetic Analysis of Hydroxamate Inhibitor Binding—The involvement of MMPs in the breakdown and remodeling of the connective tissue under pathological conditions such as arthritis and cancer makes them attractive targets for the development of specific inhibitors for therapeutic intervention. In recent years, hydroxamic acid-based peptide inhibitors were developed, which react with 1:1 stoichiometry with MMPs, as revealed by x-ray crystallography (33, 34). The apparent K_i values for the inhibition of active $\Delta_{260-508}$ MMP-19 with the inhibitors BB-94 (British Biotech), CT-1746 (Celltech), and Ro31-9790 (Hoffmann-La Roche) were determined (Table III). Only the K_i^{app} for Ro30-9790 was determined with accuracy (1.22 nM), since its value is above the employed enzyme concentration, whereas the values obtained for the other two in-

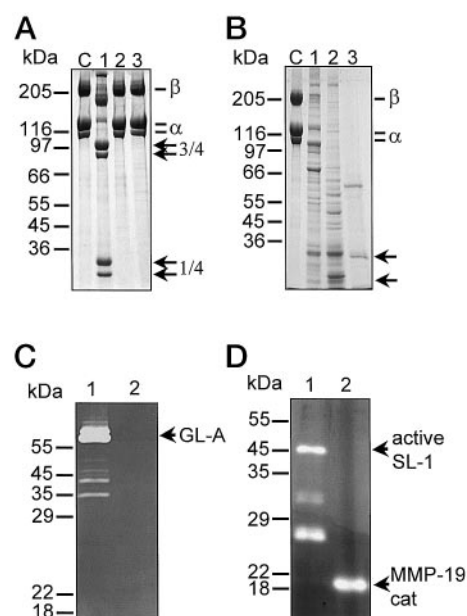


FIG. 4. SDS-PAGE (6%) analysis: time-dependent hydrolysis of type I collagen (A) and gelatin (B) by active $\Delta_{260-508}$ MMP-19, and analysis of $\Delta_{260-508}$ MMP-19 activity by zymography (C and D). Panel A, type I collagen, incubated for 24 h at room temperature with: lane 1, human neutrophil collagenase (MMP-8); lane 2, active full-length MMP-19 (from NS0); lane 3, active $\Delta_{260-508}$ MMP-19. Panel B, type I gelatin, incubated for 24 h at room temperature with: lane 1, active $\Delta_{260-508}$ MMP-19; lane 2, stromelysin-1 (MMP-3); lane 3, gelatinase A (MMP-2). The original proteins are marked with a dash and the major cleavage products with arrows on the right. Stromelysin-1 was activated with trypsin, and human neutrophil collagenase was activated with APMA. The enzyme/substrate ratio used in these assays was 1/10 (w/w). Controls (C) were incubated under the same conditions in the presence of EDTA for 24 h. Panel C, gelatin zymogram; lane 1, active gelatinase A (10 ng); lane 2, active $\Delta_{260-508}$ MMP-19 (100 ng). Panel D, casein zymogram; lane 1, active stromelysin-1 (10 ng); lane 2, active $\Delta_{260-508}$ MMP-19 (10 ng). Molecular mass markers are indicated on the left of each gel.

hibitors were both in the low picomolar range and therefore must be regarded as rough estimates of the real values. Interestingly, the K_i^{app} value for the inhibition of stromelysin-1 (MMP-3) with Ro31-9790 (119 nM) is about 100 times higher than our value determined for $\Delta_{260-508}$ MMP-19. In addition, the other two synthetic compounds tested seem also to inhibit $\Delta_{260-508}$ MMP-19 more efficiently than stromelysin-1, suggesting that the architectures of the active sites of these two enzymes, responsible for inhibitor interactions, are different (Table III).

Hydrolysis of Extracellular Matrix Components—A large variety of extracellular matrix components, purified from different connective tissues, were incubated with the catalytic domain of MMP-19 in time-course experiments prior to SDS-PAGE analysis to study its substrate specificity and to evaluate its possible function *in vivo* (Figs. 4–8). These experiments were also performed using stromelysin-1 as a comparison, since active $\Delta_{260-508}$ MMP-19 exhibits similar specificity toward the synthetic fluorescent peptide substrate Mca-Pro-Leu-Ala-Nva-Dpa-Ala-Arg-NH₂ (Table I).

As expected, collagen type I was resistant to hydrolysis by the catalytic domain of MMP-19 (Fig. 4A). However, full-length MMP-19 purified from the medium of stable transfected NS0 cells was also unable to cleave triple-helical collagen. Furthermore, catalytic domain and full-length MMP-19 exhibit similar activity *versus* gelatin (data not shown). Our data show that the influence of the COOH terminus on MMP-19 substrate specificity is negligible for the substrates studied, that the enzyme is non-collagenolytic, and thus the catalytic domain

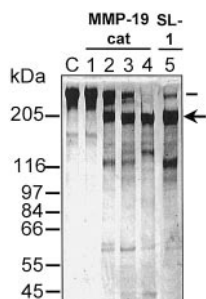


FIG. 5. SDS-PAGE (6%) analysis: time-dependent hydrolysis of the large tenascin-C isoform by active $\Delta_{260-508}$ MMP-19. Figure shows large tenascin-C isoform, incubated at 37 °C with active $\Delta_{260-508}$ MMP-19 and stromelysin-1. Incubation times were as follows: lane 1, 0 h; lane 2, 3 h; lane 3, 6 h; lanes 4 and 5, 24 h. The original protein is marked with a dash and the major cleavage product with an arrow on the right. Stromelysin-1 was activated with trypsin. The enzyme/substrate ratio used in the assays was 1/10 (w/w). The control (C) was incubated under the same conditions in the presence of EDTA for 24 h. Molecular mass markers are indicated on the left of the gel.

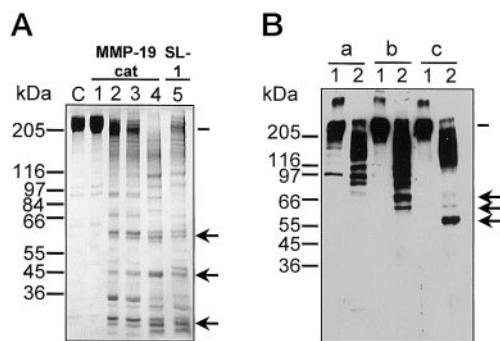


FIG. 6. SDS-PAGE (A) and Western blot (B) analysis of fibronectin hydrolysis by active $\Delta_{260-508}$ MMP-19 at 37 °C for 24 h. Panel A, SDS-PAGE (6%) analysis: time-dependent hydrolysis (0–24 h) of fibronectin by active $\Delta_{260-508}$ MMP-19 (lanes 1–4); for comparison, fibronectin was incubated with trypsin activated stromelysin-1 for 24 h (lane 5). Incubation times were as follows: lane 1, 0 h; lane 2, 3 h; lane 3, 6 h; lanes 4 and 5, 24 h. Panel B, Western blot analysis. Lanes 1, control; lanes 2, fibronectin incubated in the presence of $\Delta_{260-508}$ MMP-19 for 24 h. Pair a, monoclonal antibody recognizing an epitope near the gelatin binding region (clone III); pair b, monoclonal antibody directed against an epitope in the central cell-binding region (clone II); pair c, monoclonal antibody directed to an epitope near the COOH-terminal heparin-binding domain (clone I). The original proteins are marked with a dash and the major cleavage products with arrows on the right of each gel. The enzyme/substrate ratio used in these assays was 1/10 (w/w). Controls were incubated under the same conditions in the presence of EDTA for 24 h. Molecular mass markers are indicated on the left of each gel.

represents a good model to study macromolecular substrate hydrolysis.

The catalytic domain of MMP-19 was able to degrade gelatin efficiently (Fig. 4B). However, at equivalent substrate/enzyme ratios (w/w), stromelysin-1 (MMP-3) and gelatinase A (MMP-2) display a considerably higher activity against this macromolecule, if analyzed by SDS-PAGE (Fig. 4B). Although $\Delta_{260-508}$ MMP-19 degraded gelatin, hydrolysis is not sufficient to generate a definable zone of lysis using gelatin zymography presumably due to the large mass of the generated fragments. Thus, it is not possible to use gelatin zymography to detect MMP-19 activity (Fig. 4C). In contrast, casein is hydrolyzed efficiently and $\Delta_{260-508}$ MMP-19 activity can therefore be monitored using casein zymograms (Fig. 4D). In comparison to $\Delta_{260-508}$ MMP-19, stromelysin-1 hydrolyzes gelatin and can therefore be analyzed by gelatin zymography. In addition, the specific activity of MMP-19 catalytic domain was assessed using 14 C-labeled gelatin and casein (17). In this assay, the en-

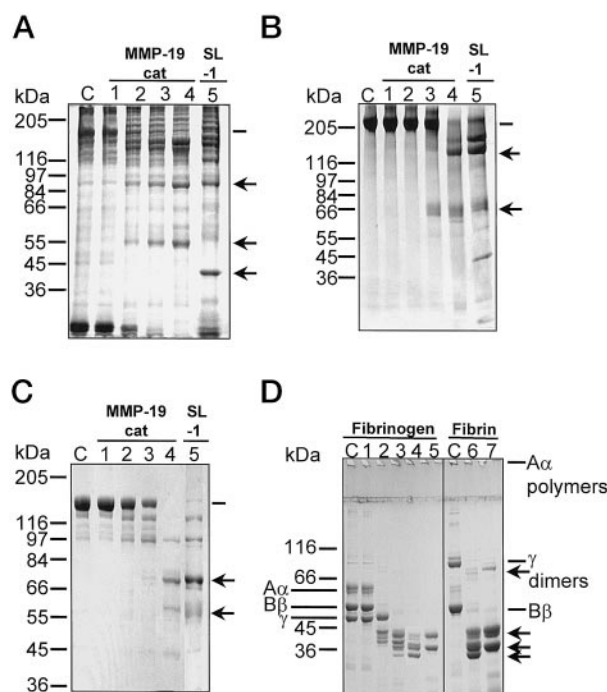


FIG. 7. SDS-PAGE (6%) analysis: time-dependent hydrolysis of the basement membrane components type IV collagen (A), laminin (B), and nidogen (C), and fibrinogen and fibrin (D) by active $\Delta_{260-508}$ MMP-19 at 37 °C. The original proteins are marked with a dash (fibrinogen, left side; fibrin, right side of the gel) and the major cleavage products with arrows. For comparison, the above ECM molecules were incubated with trypsin-activated stromelysin-1 for 24 h (panel D, lanes 5 and 7). In panels A, B, and C, incubation times were as follows: lane 1, 0 h; lane 2, 3 h; lane 3, 6 h; lanes 4 and 5, 24 h. Incubation times in panel D were as follows: lane 1, 0 h; lane 2, 1 h; lane 3, 5 h; lanes 4–7, 24 h. The enzyme/substrate ratio used was 1/10 (w/w) in all assays. Controls were incubated under the same conditions in the presence of EDTA for 24 h. Molecular mass markers are indicated on the left of each gel.

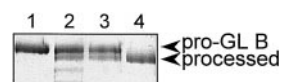


FIG. 8. SDS-PAGE (8%) analysis: processing of latent human gelatinase B (MMP-9) by active $\Delta_{260-508}$ MMP-19 at 37 °C in time-dependent fashion. Incubation times were as follows: lane 1, 0 h; lane 2, 3.5 h; lane 3, 5 h; lane 4, 24 h. The enzyme/substrate ratio used in the assay was 1/10 (w/w). Controls were incubated under the same conditions in the presence of EDTA for 24 h (data not shown).

zyme was able to hydrolyze gelatin with a specific activity of 78.45 units/ μ mol and casein with 8491 units/ μ mol. In comparison, the specific activities for the hydrolysis of gelatin by stromelysin-1 and gelatinase A are 2 to 4 orders of magnitude higher than observed for $\Delta_{260-508}$ MMP-19, respectively (20, 21). On the other hand, specific activities of $\Delta_{260-508}$ MMP-19 and stromelysin-1 for the hydrolysis of casein are similar (20).

The two different isoforms of human tenascin-C were incubated with the MMP-19 catalytic domain (Fig. 5) (35). Analysis of the reaction products revealed that the small isoform was resistant (data not shown), as expected (18), while the large tenascin-C isoform was cleaved into two high molecular mass fragments displaying masses of 190 and 120 kDa. The cleavage pattern is identical to the one generated by stromelysin-1 under the same conditions, but MMP-19 seems to be more effective in processing the large isoform of tenascin-C. In addition, it was demonstrated that MMP-19 catalytic domain is able to hydrolyze the large isoform to the same sized products as gelatinase A (18).

Fibronectin was degraded by MMP-19 catalytic domain in a

time-dependent manner (Fig. 6). Several fragments of 200, 160, 110, 100, 95, 80, 60, 45, 35, and 25 kDa were generated. Initially, fragments of 200, 160, 95, 80, 60, 35, and 25 kDa were produced after 2 h of incubation, and fragments of 160, 100, 60, 45, and 25 kDa were the final products (Fig. 6A). The cleavage products after 24 h of incubation were identical to those generated by stromelysin-1; however, active $\Delta_{260-508}$ MMP-19 was more efficient in cleaving fibronectin. The fibronectin degradation products generated by active $\Delta_{260-508}$ MMP-19 were characterized by immunoblotting using monoclonal antibodies against three different epitopes of the 220-kDa molecule (Fig. 6B). Three different bands, of 75, 64, and 60 kDa, were recognized by the antibody against the COOH-terminal heparin-binding domain (clone I). The larger two of these bands were also seen by the antibody raised against the central cell binding domain (clone II), but not by the antibody against the NH₂-terminal gelatin-binding domain (clone III) of fibronectin, suggesting preferential processing within the NH₂-terminal region of the molecule. Furthermore, clones II and III both detect bands of 110, 95, and 90 kDa. Interestingly, proteolytic fibronectin fragments have been shown to block fibronectin receptors, decrease cell attachment, and alter cell migration and therefore contribute to cell-regulatory processes (36). Fragments containing cell binding and heparin binding domains (75 and 64 kDa) may interfere with cell-proteoglycan interactions. In addition, fragments of fibronectin have been suggested to be involved in the induction of specific genes, such as proteases required for ECM remodeling (37). However, further studies are required to determine the possible function of fibronectin fragments generated by MMP-19 on cell attachment and cell migration.

Since MMP-19 was found in blood vessels in the synovium of RA patients, as well as in healthy skin and uterine ligaments, and therefore implicated in angiogenesis, degradation of basement membrane components was examined (Fig. 7) (7, 8). In contrast to triple-helical collagen type I, collagen type IV, a major component of basement membranes consisting of two α_1 (IV) chains and one α_2 (IV) chain, was cleaved into two main high molecular mass fragments with molecular masses of 94 and 56 kDa in addition to some minor fragments (Fig. 7A). Stromelysin-1 generates two bands with masses of 42 and 94 kDa, which indicates a different specificity *versus* this molecule (Fig. 7A). Interestingly, MMP-19 was found to be co-expressed with collagen type IV in the tunica media of blood vessels of RA synovium (8). Laminin, a heterotrimer with an α -, β -, and γ -chain (205, 215, and 400 kDa, respectively), was hydrolyzed by MMP-19 catalytic domain after 24 h to two major products with molecular masses of 64 and 140 kDa (Fig. 7B). The same cleavage products occur during hydrolysis with stromelysin-1 but not with the catalytic domain of MT1-MMP (38). However, under these conditions, the catalytic domain of MMP-19 seems to be more effective toward laminin than stromelysin-1. Nidogen, a basement membrane component with a mass of 158 kDa, was degraded by active $\Delta_{260-508}$ MMP-19 (Fig. 7C). The bands generated after a 24-h incubation had molecular mass values of 98, 72, and 60 kDa with a clear cleavage pattern, which was similar to the one generated by stromelysin-1. Like laminin, nidogen seemed to be degraded more efficiently by $\Delta_{260-508}$ MMP-19 than by stromelysin-1. Nidogen binds to laminin, type IV collagen, and proteoglycans and facilitates a build-up of the basement membrane's network (39). Thus, our results suggest that MMP-19 may be a potent player in the degradation of basement membrane components. We have demonstrated that type IV collagen, laminin, as well as nidogen are efficiently hydrolyzed by MMP-19, and, in conjunction with its expression in the tunica media, the enzyme may have

a role during angiogenesis (7). To further investigate the ability of MMP-19 to hydrolyze ECM components, $\Delta_{260-508}$ MMP-19 was incubated with fibrinogen and fibrin, both molecules with a distinct role during new blood vessel formation (Fig. 7D). The cleavage pattern showed complete hydrolysis of the fibrinogen A α and B β chains after 1 h and loss of the γ chain after 5 h of incubation. After 24 h, fragments of sizes between 35 and 42 kDa seem to represent the final cleavage products. Fibrin was hydrolyzed by MMP-19 catalytic domain in a similar fashion to fibrinogen, resulting in three major cleavage products between 35 and 42 kDa and a double band at 72 kDa, which appeared to be derived from the γ dimers (19). In comparison, hydrolysis of fibrinogen and fibrin by stromelysin-1 for 24 h resulted in only two distinct fragments of approximately 42 and 37 kDa, whereas, in case of fibrin, a doublet at 42 kDa was obtained (Fig. 7D).

Activation of Other Pro-matrix Metalloproteinases—MMPs have been implicated in the activation and hydrolysis of secreted or membrane-bound proteinases (e.g. other MMPs) and precursors of growth factors (40, 41). Thus, in order to determine the possible role of MMP-19 upon activation of other MMPs, we incubated various proMMPs (MMP-1, -2, -3, -8, -9, -13, and -14) with active $\Delta_{260-508}$ MMP-19. However, only human progelatinase B (MMP-9) was processed by the enzyme in a time-dependent fashion generating a final form of M_r 82,000 after 24 h of incubation when analyzed by SDS-PAGE (Fig. 8). The MMP-19 catalytic domain was not able to process any of the other MMPs tested (MMP-1, -2, -3, -13, and -14; data not shown). The processed form of human gelatinase B does not show hydrolytic activity against the synthetic quenched fluorescent substrate Mca-Pro-Leu-Gly-Dpa-Ala-Arg-NH₂. NH₂-terminal sequencing revealed that $\Delta_{260-508}$ MMP-19 cleaves the Lys⁷³-Ala⁷⁴ bond upstream of the . . . PRCGVPD . . . sequence within the propeptide region of MMP-9, leaving its latency motif intact. This cleavage may induce conformational changes in the propeptide exposing the final activation site (Arg⁸⁷-Phe⁸⁸) to be hydrolyzed by a second proteolysis, which can not be performed by MMP-19 (42).

Relatively high levels of MMP-19 expression were detected by Northern blot analysis in a wide variety of normal tissues (4). This pattern of expression is unusual for MMPs, which are not constantly produced by adult cells but are mostly induced during physiological conditions associated with extensive connective tissue remodeling, such as wound healing, uterine postpartum involution, or mammary gland involution. Therefore, MMP-19 may be involved in normal ECM remodeling processes. Interestingly, MT1-MMP (MMP-14) shows an expression pattern similar to that of MMP-19 and is regarded as major player in surface activation of other MMPs and ECM remodeling (43–46).

This work represents the first detailed characterization of the enzymatic properties of MMP-19; our studies have revealed the enzyme's tendency to autoactivate, a potent activity on a wide variety of ECM substrates, and evidence about TIMP interaction.

REFERENCES

- Nagase, H., and Woessner, J. F., Jr. (1999) *J. Biol. Chem.* **274**, 21491–21494
- Reynolds, J. J., and Meikle, M. C. (1997) *Periodontology* **2000** **14**, 144–157
- Yong, V. W., Krekoski, C. A., Forsyth, P. A., Bell, R., and Edwards, D. R. (1998) *Trends Neurosci.* **21**, 75–80
- Pendás, A. M., Knäuper, V., Puente, X. S., Llano, E., Mattei, M. G., Apte, S., Murphy, G., and López-Otin, C. (1997) *J. Biol. Chem.* **272**, 4281–4286
- Konttinen, Y. T., Ainola, M., Valleala, H., Ma, J., Ida, H., Mandelin, J., Kinne, R. W., Santavirta, S., Sorsa, T., López-Otin, C., Takagi, M. (1999) *Ann. Rheum. Dis.* **58**, 691–697
- Sedlacek, R., Mauch, S., Kolb, B., Schätzlein, C., Eibel, H., Peter, H. H., Schmitt, J., and Krawinkel, U. (1998) *Immunobiology* **198**, 408–423
- Kolb, C., Mauch, S., Peter, H. H., Krawinkel, U., and Sedlacek, R. (1997) *Immunol. Lett.* **57**, 83–88
- Kolb, C., Mauch, S., Krawinkel, U., and Sedlacek, R. (1999) *Exp. Cell Res.* **250**,

- 122–130
9. Ho, S. N., Hunt, H. D., Horton, R. M., Pullen, J. K., and Pease, L. R. (1989) *Gene (Amst.)* **77**, 51–59
 10. Crabbe, T., Willenbrock, F., Eaton, D., Hynds, P., Carne, A. F., Murphy, G., and Docherty, A. J. P. (1992) *Biochemistry* **31**, 8500–8507
 11. Murphy, G., Houbrechts, A., Cockett, M. I., Williamson, R. A., O'Shea, M., and Docherty, A. J. P. (1991) *Biochemistry* **30**, 8097–8102
 12. Willenbrock, F., Crabbe, T., Slocombe, P. M., Sutton, C. W., Docherty, A. J. P., Cockett, M. I., O'Shea, M., Brocklehurst, K., Phillips, I. R., and Murphy, G. (1993) *Biochemistry* **32**, 4330–4337
 13. Apte, S. S., Olsen, B. R., and Murphy, G. (1995) *J. Biol. Chem.* **270**, 14313–14318
 14. Wingfield, P. T., Sax, J. K., Stahl, S. J., Kaufman, J., Palmer, I., Chung, V., Corcoran, M. L., Kleiner, D. E., and Stetler-Stevenson, W. G. (1999) *J. Biol. Chem.* **274**, 21362–21368
 15. Butler, G. S., Hutton, M., Wattam, B. A., Williamson, R. A., Knäuper, V., Willenbrock, F., and Murphy, G. (1999) *J. Biol. Chem.* **274**, 20391–20396
 16. Knight, C. G., Willenbrock, F., and Murphy, G. (1992) *FEBS Lett.* **296**, 263–266
 17. Cawston, T. E., and Barrett, A. J. (1979) *Anal. Biochem.* **99**, 340–345
 18. Siri, A., Knäuper, V., Veirana, N., Caocci, F., Murphy, G., and Zardi, L. (1995) *J. Biol. Chem.* **270**, 8650–8654
 19. Bini, A., Itoh, Y., Kudryk, B. J., and Nagase, H. (1996) *Biochemistry* **35**, 13056–13063
 20. Koklitis, P. A., Murphy, G., Sutton, C., and Angal, S. (1991) *Biochem. J.* **276**, 217–221
 21. Murphy, G., Cockett, M. I., Ward, R. V., and Docherty, A. J. P. (1991) *Biochem. J.* **277**, 277–279
 22. Quesada, A. R., Barbacid, M. M., Mira, E., Fernández-Resa, P., Márquez, G., and Aracil, M. (1997) *Clin. Exp. Metastasis* **15**, 26–32
 23. Park, A. J., Matrisian, L. M., Kells, A. F., Pearson, R., Yuan, Z., and Navre, M. (1991) *J. Biol. Chem.* **266**, 1584–1590
 24. Holman, C. M., Kan, C. C., Gehring, M. R., and Van, W. H. (1999) *Biochemistry* **38**, 677–681
 25. Nguyen, Q., Willenbrock, F., Cockett, M. I., O'Shea, M., Docherty, A. J. P., and Murphy, G. (1994) *Biochemistry* **33**, 2089–2095
 26. Greene, J., Wang, M. S., Liu, Y. L. E., Raymond, L. A., Rosen, C., and Shi, Y. N. E. (1996) *J. Biol. Chem.* **271**, 30375–30380
 27. Fernandez-Catalan, C., Bode, W., Huber, R., Turk, D., Calvete, J. J., Lichte, A., Tschesche, H., and Maskos, K. (1998) *EMBO J.* **17**, 5238–5248
 28. Muskett, F. W., Frenkiel, T. A., Feeney, J., Freedman, R. B., Carr, M. D., and Williamson, R. A. (1998) *J. Biol. Chem.* **273**, 21736–21743
 29. Meng, Q., Malinovkii, V., Huang, W., Hu, Y., Chung, L., Nagase, H., Bode, W., Maskos, K., and Brew, K. (1999) *J. Biol. Chem.* **274**, 10184–10189
 30. Nagase, H., Suzuki, K., Cawston, T. E., and Brew, K. (1997) *Biochem. J.* **325**, 163–167
 31. Huang, W., Meng, Q., Suzuki, K., Nagase, H., and Brew, K. (1997) *J. Biol. Chem.* **272**, 22086–22091
 32. Gomis-Rüth, F.-X., Maskos, K., Betz, M., Bergner, A., Huber, R., Suzuki, K., Yoshida, N., Nagase, H., Brew, K., Bourenkov, G. P., Bartunik, H., and Bode, W. (1997) *Nature* **389**, 77–79
 33. Becker, J. W., Marcy, A. I., Rokosz, L. L., Axel, M. G., Burbaum, J. J., Fitzgerald, P. M. D., Cameron, P. M., Esser, C. K., Hagmann, W. K., Hermes, J. D., and Springer, J. P. (1995) *Protein Sci.* **4**, 1966–1976
 34. Lovejoy, B., Welch, A. R., Carr, S., Luong, C., Broka, C., Hendricks, R. T., Campbell, J. A., Walker, K. A., Martin, R., Van, W. H., and Browner, M. F. (1999) *Nat. Struct. Biol.* **6**, 217–221
 35. Savarese, J. J., Erickson, H., and Scully, S. P. (1996) *J. Orthop. Res.* **14**, 273–281
 36. Von Bredow, D. C., Nagle, R. B., Bowden, G. T., and Cress, A. E. (1995) *Exp. Cell Res.* **221**, 83–91
 37. Homandberg, G. A., Meyers, R., and Xie, D. (1992) *J. Biol. Chem.* **267**, 3597–3604
 38. D'Ortho, M.-P., Will, H., Atkinson, S., Butler, G. S., Messent, A., Gavrilovic, J., Smith, B., Timpl, R., Zardi, L., and Murphy, G. (1997) *Eur. J. Biochem.* **250**, 751–757
 39. Mayer, U., Kohfeldt, E., and Timpl, R. (1998) *Ann. N. Y. Acad. Sci.* **857**, 130–142
 40. Massague, J., Pandiella, A. (1993) *Annu. Rev. Biochem.* **62**, 515–541
 41. Gearing, A. J. H., Beckett, P., Christodoulou, M., Churchill, M., Clements, J., Davidson, A. H., Drummond, A. H., Galloway, W. A., Gilbert, R., Gordon, J. L., Leber, T. M., Managan, M., et al. (1994) *Nature* **370**, 555–557
 42. Sang, Q. X., Birkedal-Hansen, H., and Van Wart, H. E. (1995) *Biochim. Biophys. Acta* **1251**, 99–108
 43. Holmbeck, K., Bianco, P., Caterina, J., Yamada, S., Kromer, M., Kuznetsov, S. A., Mankani, M., Robey, P. G., Poole, A. R., Pidoux, I., Ward, J. M., and Birkedal-Hansen, H. (1999) *Cell* **99**, 81–92
 44. Will, H., and Hinzmann, B. (1995) *Eur. J. Biochem.* **231**, 602–608
 45. Takino, T., Sato, H., Shinagawa, A., and Seiki, M. (1995) *J. Biol. Chem.* **270**, 23013–23020
 46. Knäuper, V., Murphy, G., and Tschesche, H. (1996) *Eur. J. Biochem.* **235**, 187–191